

seq-JEPA: Autoregressive Predictive Learning of Invariant-Equivariant World Models

Hafez Ghaemi^{1 2 3} Etilf B. Muller^{*} ^{1 2 3} Shahab Bakhtiari^{*} ^{1 2}

Abstract

Current self-supervised algorithms mostly rely on transformations such as data augmentation and masking to learn visual representations. This is achieved by inducing invariance or equivariance with respect to these transformations after encoding two views of an image. This dominant two-view paradigm can limit the flexibility of learned representations for downstream adaptation by creating performance trade-offs between invariance-related tasks such as image classification and more fine-grained equivariance-related tasks. In this work, we introduce *seq-JEPA*, a world modeling paradigm based on joint-embedding predictive architecture that leverages architectural inductive biases to resolve this trade-off. Without requiring an additional equivariance predictor or loss term, *seq-JEPA* simultaneously learns two architecturally segregated representations: one equivariant to the specified transformations and another invariant to them and suited for tasks such as classification. To do so, our model processes a short sequence of different views (observations) of an input image. Each encoded view is concatenated with embeddings corresponding to the relative transformation (action) producing the next observation in the sequence. A transformer encoder outputs an aggregate representation of this sequence, which is subsequently conditioned on the action leading to the next observation to predict its representation. Empirically, *seq-JEPA* achieves strong performance on equivariant benchmarks and image classification without sacrificing one for the other. Additionally, our framework excels at tasks that inherently require aggregating a sequence of observations, such as path integration across actions and predictive learning across eye movements.

^{*}Equal contribution ¹Université de Montréal ²Mila ³Centre de Recherche Azrieli du CHU Sainte-Justine. Correspondence to: Hafez Ghaemi <hafez.ghaemi@umontreal.ca>.

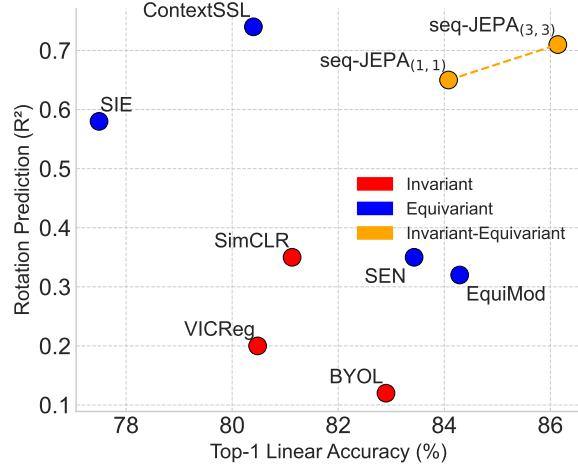


Figure 1: Top-1 linear classification (invariance) versus rotation prediction (equivariance) performance on 3DIEBench. Our world model, seqJEPA, learns representations for both invariance- and equivariance-related tasks at the same time. Subscripts indicate training and inference sequence lengths used in seq-JEPA.

1. Introduction

Self-supervised learning (SSL) in latent space has made significant progress in visual representation learning in recent years, closing the gap with supervised learning in many downstream tasks (van den Oord et al., 2019; Misra & van der Maaten, 2020; He et al., 2020; Chen et al., 2020; Grill et al., 2020; Chen & He, 2021; Caron et al., 2020; 2021; Zbontar et al., 2021; Bardes et al., 2022; Baevski et al., 2022; Assran et al., 2023). Most SSL methods learn their representations by comparing two transformed views of a sample image and inducing invariance with respect to these transformations (Chen et al., 2020; He et al., 2020; Dwibedi et al., 2021; HaoChen et al., 2021; Yeh et al., 2022; Caron et al., 2020; 2021; Ermolov et al., 2021; Assran et al., 2022; Zbontar et al., 2021; Bardes et al., 2022). Another group of methods employ techniques to preserve some information about the transformations and learn equivariant representations (Lee et al., 2021; Xiao et al., 2021; Park et al., 2022; Dangovski et al., 2022; Gupta et al., 2023;

Garrido et al., 2023; 2024; Gupta et al., 2024; Yerxa et al., 2024).

Equivariance is a required representational property for many fine-grained downstream tasks. For example, given representations that are invariant to color, it is not possible to distinguish between certain species of flowers or birds (Lee et al., 2021; Xiao et al., 2021). Additionally, recent work has shown that equivariant representations are better aligned with neural responses in primate visual cortex and could be important for building more accurate models thereof (Yerxa et al., 2024). Although some of the equivariant SSL methods have empirically shown a slight performance improvement in downstream tasks traditionally associated with invariance (e.g., image classification) (Devillers & Lefort, 2022; Park et al., 2022; Gupta et al., 2023), recent studies have revealed a persistent trade-off between invariance and equivariance in self-supervised representation learning (Garrido et al., 2023; 2024; Gupta et al., 2024; Yerxa et al., 2024). The existence of such a trade-off has been recently supported by theoretical arguments (Wang et al., 2024), highlighting the need for innovative architectural and objective design to mitigate it.

Humans and other animals rely on a *sequence* of actions and consequent observations (views) for developing appropriate visual representation during novel object learning (Harman et al., 1999; Vuilleumier et al., 2002). For example, they recognize a 3-D object by changing their viewpoint and examining different sides of the object (Tarr et al., 1998). Inspired by this, we introduce seq-JEPA, a world modeling paradigm based on joint-embedding predictive architecture (LeCun, 2022; Dawid & LeCun, 2024) that leverages architectural inductive biases to enable such sequential processing in SSL and resolve the invariance-equivariance trade-off. Our model simultaneously learns two architecturally distinct representations: one equivariant to a specified set of transformations and another suited for invariance-related tasks, such as image classification.

Specifically, our framework (Figure 2) processes a short sequence of different views (observations) of an input image. Each encoded view is concatenated with embeddings corresponding to the relative transformation (action) that produces the next observation in the sequence. These concatenated representations are then fed to a transformer encoder, resembling working memory, that outputs an aggregate representation, which is subsequently conditioned on the action leading to the next observation and used to predict its representation.

Our results show that the encoded views in seq-JEPA become transformation/action-equivariant. Through ablation experiments, we show that action conditioning plays a key role in promoting equivariant representation learning in the encoder network. In contrast, the aggregate representation

of views, produced at the output of the sequence transformer, becomes largely transformation/action-invariant. This architectural disentanglement of invariant and equivariant representations in seq-JEPA is key to the competitive performance of our model compared to both invariant and equivariant SSL methods (Figure 1). We empirically demonstrate this advantage across multiple tasks and benchmarks. It is important to emphasize that, unlike many previous approaches in equivariant SSL (Lee et al., 2021; Park et al., 2022; Dangovski et al., 2022; Gupta et al., 2023; Garrido et al., 2023; Gupta et al., 2024; Yerxa et al., 2024), neither our objective function nor our architecture explicitly encourages the learning of invariant-equivariant representations. Instead, the learning of invariance and equivariance, along with their architectural separation, emerges as an implicit consequence of action-conditioned sequential predictive learning and the model architecture.

Furthermore, we explore other benefits of moving away from the dominant two-view paradigm in SSL and demonstrate that seq-JEPA is capable of solving tasks that inherently require aggregating a sequence of observations. In one scenario, inspired by embodied vision in primates, our model learns image representations without hand-crafted augmentations or masking, solely via predictive learning across simulated saccades (eye movements). Finally, seq-JEPA is also capable of path integration over a sequence of actions such as eye movements in the previously described scenario, or 3-D object rotations in 3DIEBench (Garrido et al., 2023). A summary of our contributions are as follows:

- We propose seq-JEPA, a self-supervised world model that leverages a sequence of action-observation pairs to learn separate representations for equivariance- and invariance-demanding downstream tasks without requiring an additional equivariance predictor or loss term.
- We empirically show the effectiveness of our world modeling paradigm in comparison with invariant and equivariant SSL methods on both invariance- and equivariance-related benchmarks without sacrificing one for the other.
- We demonstrate that seq-JEPA is capable of solving tasks that inherently require aggregating a sequence of observations, such as path integration across actions and predictive learning across eye movements.

2. Method

2.1. Invariant and equivariant representations

Before describing the architecture and training procedure of seq-JEPA, we provide the nomenclature of invariant and equivariant representation learning in SSL (Dangovski et al.,

2022; Devillers & Lefort, 2022). Consider \mathcal{T} as a distribution of possible data transformations that is parametrized by a vector t . These transformations can be any type of hand-crafted data augmentation, such as geometric transformations or masking, that transform an original data point x to different views. For example, we denote x_1 and x_2 as views generated from x via two transformations t_1 and t_2 sampled from \mathcal{T} . Additionally, we denote a as a transformation that transforms x_1 to x_2 . Here, we distinguish between t and a , and call t a transformation and a an action, i.e., a *relative* transformation that transforms x_1 to x_2 . Furthermore, we denote f as an encoder function that projects the data space into a latent space. Given a transformation t , the encoder and its representations are said to be equivariant to t if

$$\forall t \in \mathcal{T}, \exists u_t \text{ s.t. } f(t(x)) = u_t(f(x)). \quad (1)$$

We can also define equivariance given the action a and two views x_1 and x_2 as

$$\forall a \in \mathcal{T}, \exists u_a \text{ s.t. } f(x_2) = u_a(f(x_1)), \quad (2)$$

where u_t and u_a are functions that produce displacements in latent space corresponding to their associated transformation/action. As a special case of equivariance, the encoder and its representations are said to be invariant to t if u_t and u_a are identity functions, i.e., $f(t(x)) = f(x)$ or $f(x_2) = f(x_1)$.

2.2. Architecture

The overall architecture of seq-JEPA is depicted in Figure 2. Denote $\{x_i\}_{i=1}^{M+1}$ as a sequence of views generated from a data sample x using transformations $\{t_i\}_{i=1}^{M+1}$. The corresponding actions (relative transformations), whose embeddings are learned via a linear layer are denoted as $\{a_i\}_{i=1}^M$. A backbone encoder, f_θ encodes the first M views and produces representations $\{z_i\}_{i=1}^M$. These representations, except for z_M , are concatenated with their corresponding action embeddings and fed to a sequence model, e.g., a transformer encoder, g_ϕ (no MLP projector is used after the encoder). This transformer module is tasked with aggregating the sequence of representations of action-observation pairs to produce an aggregate representation. We use a learnable token which we call $[\text{AGG}]$ to learn the aggregate representation (this token resembles a $[\text{CLS}]$ token in vision transformers (Dosovitskiy et al., 2020)). The output corresponding to $[\text{AGG}]$ is therefore:

$$z_{\text{AGG}} = g_\phi((z_1, a_1), (z_2, a_2), \dots, (z_{M-1}, a_{M-1}), z_M) \quad (3)$$

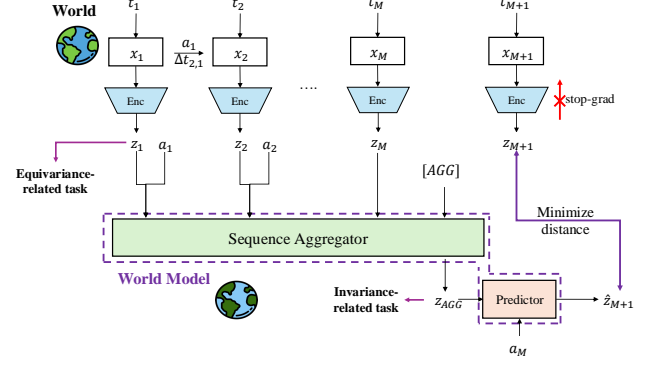


Figure 2: Overview of the proposed architecture; seq-JEPA is a world modeling paradigm that leverages a sequence of action-observation pairs to learn separate representations for equivariance- and invariance-related tasks.

The representation z_{AGG} is subsequently concatenated with the last action embedding a_M which corresponds to the relative transformation between x_M and x_{M+1} , and is fed to an MLP predictor module h_ψ to predict the representation of x_{M+1} , i.e., $\hat{z}_{M+1} = h_\psi(z_{\text{AGG}}, a_M)$. The last view x_{M+1} , is itself encoded using a target encoder whose weights are an exponential moving average (EMA) of the encoder f_θ used to encode the sequence of observations. The representation z_{M+1} is passed through an stop-gradient (sg) to prevent representational collapse. Our objective is then to maximize the cosine similarity between \hat{z}_{M+1} and z_{M+1} , which we achieve by minimizing the following prediction loss,

$$\mathcal{L}_{\text{seq-JEPA}} = 1 - \frac{\hat{z}_{M+1}}{\|\hat{z}_{M+1}\|_2} \cdot \frac{\text{sg}(z_{M+1})}{\|\text{sg}(z_{M+1})\|_2}. \quad (4)$$

No additional equivariance predictor or loss function is used when training the framework.

2.3. Action and observation sets

In order to evaluate our model and measure its ability to generalize to different types of transformations, we consider three distinct sets of transformation and their corresponding action-observation pairs (Figure 3a). Descriptions of each transformation set are provided below, with additional details available in Section A.1.

3D Invariant Equivariant Benchmark (3DIEBench). We use the 3DIEBench dataset (Garrido et al., 2023) as our first evaluation benchmark. This dataset is specifically designed for measuring equivariance and provides 3D object renderings with different object rotations and floor hue and lighting angles and their corresponding parameters. We specifically study equivariance to the 3D rotation group ($SO(3)$) and further to floor and light hue in this benchmark.

Hand-crafted data augmentations. In this setting, observations are transformed image views generated by hand-crafted augmentations that are typically used in the two-view paradigm of SSL. The actions are relative augmentation parameters between two views. We measure equivariance to crop, color jitter, and blur transformations. As benchmarks for this setting, we use CIFAR100 and Tiny ImageNet datasets. To generate augmented views, we follow EquiMod’s augmentation strategy (Devillers & Lefort, 2022). For details on augmentations and the corresponding parameterization, see Section A.1.

Predictive learning across saccades. Going beyond transformations such as augmentations and rotation, we explore other ways of leveraging sequential observations to learn visual representations. Specifically, we designed a procedure to learn image representations without using any hand-crafted augmentations with a similar flavor to I-JEPA (Assran et al., 2023) but without dependence on masking. Our approach is enabled by seq-JEPA’s architecture and its ability to produce an aggregate representations from a sequence of observations. In this setting, given a full-size high-resolution image, we extract a number of smaller patches and use them as a sequence of partial observations. In our experiments with the STL-10 dataset, we use 32 by 32 patches, i.e. one-ninth of the original image.

The action in this setup corresponds to the relative position between the center of two subsequent patches, i.e. a simulated act of rapid eye movements (also known as saccades) from one point of the image to another. Although it is possible to use random positions as patch centers (fixations) for the sequence, we show that adopting two techniques inspired by embodied vision in primates improves the quality of the aggregate representation and its downstream classification performance (Figure 3b). The first technique utilizes image saliences (Itti et al., 1998; Li, 2002; Zhaoping, 2014) to sample fixations. To generate saliency maps, we use a pre-trained saliency prediction model, DeepGaze IIE (Linardos et al., 2021). Given a dataset, we pre-extract and store the saliencies without any additional overhead during training. These saliency maps can be interpreted as how likely humans are to center their gaze (fixate) on a given pixel of the image. Therefore, sampling fixations from the probability distribution corresponding to saliency maps provides more informative patches, yet similar to uniform sampling, is prone to a high degree of redundancy and overlap between patches. To remedy this, i.e. minimize overlap among patches and avoid future fixation that revisit previously attended areas, we use another technique inspired by biological vision known as inhibition of return (IoR) (Posner et al., 1985). To implement IoR, after sampling a fixation from saliency maps, we zero out the sampling probabilities of an area with a diameter equal to the patch width surrounding the previous fixations before sampling a subsequent fixation.

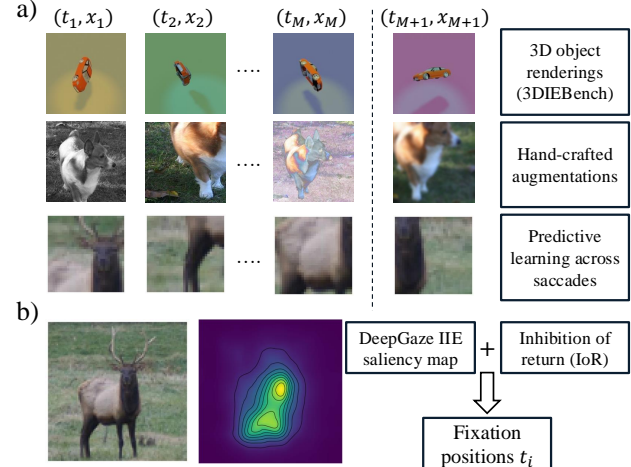


Figure 3: **a.** Types of transformations and observations used for training; seq-JEPA works with a variety of action-observation pairs such as 3D object rotations, hand-crafted augmentations, and simulated saccades. **b.** For predictive learning across saccades, image saliences and inhibition of return help create more informative and less redundant patch sequences.

In this scenario, we are interested to see whether encoder representations become sensitive to fixation positions (spatial awareness), and therefore equivariance is measured with respect to fixation coordinates.

3. Related Work

Joint-embedding predictive architectures. In JEPAs (Le-Cun, 2022; Dawid & LeCun, 2024), a predictor asymmetry is introduced in one of the two branches that traditionally encode transformed views in SSL. The representation learning task is then framed as a world modeling objective (Ha & Schmidhuber, 2018; Hafner et al., 2019), i.e., the predictor is tasked with predicting the consequence of a data transformation (action) applied to the first view that results in the second view. The predictor is conditioned on transformation parameters such as positional masks to predict the latent representation of target blocks corresponding to the masks as in I-JEPA (Assran et al., 2023), or additionally on parameters corresponding to hand-crafted image augmentations as in Image World Model (IWM) (Garrido et al., 2024). Recent works have also explored JEPAs for physical understanding (Garrido et al., 2025) and reward-free offline planning (Sobal et al., 2025).

Non-generative world models. Non-generative world models predict the consequence of an action or transformation in latent space. A line of work considers such world models in contrastive SSL by predicting the representation of a transformed view from another via a contrastive objective and

conditioned on the past or context (van den Oord et al., 2019; Gupta et al., 2024). The family of JEPAs defer the task of world modeling to a predictor module that is conditioned on the action (Assran et al., 2023; Garrido et al., 2024; Sobal et al., 2025). Non-generative world models have also garnered attention in model-based reinforcement learning (RL) and planning to improve sample efficiency (Schwarzer et al., 2021), to learn environment dynamics (Sobal et al., 2025), or to create an intrinsic novelty-based reward to improve exploration in self-predictive world models (Khetarpal et al., 2025; Ni et al., 2024; Tang et al., 2023). A prominent example of such world models is BYOL-Explore (Guo et al., 2022), in which a recurrent cell follows the encoder and is conditioned on the current action in a planning task, followed by a predictor to capture the environment’s transition dynamics.

Equivariant representation learning. Many equivariant SSL methods extend invariant methods by introducing an additional equivariance objective. This objective can be direct prediction of parameters corresponding to augmented views (Lee et al., 2021; Scherr et al., 2022; Gidaris et al., 2018; Gupta et al., 2024), or additional transformations such as rotation (Dangovski et al., 2022). EquiMod (Devillers & Lefort, 2022) and SIE (Garrido et al., 2023) predict the effect of a transformation in latent space in addition to their invariant objective. Xiao et al. (2021) use contrastive learning to train multiple projection heads for equivariance to each augmentation, where the views corresponding to the desired augmentation are considered as negative samples. In SEN (Park et al., 2022), similar to EquiMod, a predictor is used to predict the effect of transformations in latent space, yet without any invariance objective. ContextSSL (Gupta et al., 2024) learns representations that are equivariant only to the recent transformations in the current context by conditioning representations on both the current action and the past via a memory module, and further using a transformation prediction objective to avoid collapse to invariance. Another line of work including Shakerinava et al. (2022), CARE (Gupta et al., 2023), and Yerxa et al. (2024) do not assume access to transformation parameters yet require two pairs of views to which the same transformation is applied, and an equivariance loss function is minimized to induce equivariance in representations. Generative SSL methods based on masked image modeling (He et al., 2022; Bao et al., 2021; Xie et al., 2022) can become equivariant to position due to the use of positional embeddings. Finally, action-conditioned JEPAs condition the predictor on positional mask tokens (Assran et al., 2023) and augmentation parameters (Garrido et al., 2024) to induce equivariance in encoder representations without any additional equivariance objective.

Relationship to existing literature. Our framework belongs to the family of JEPAs and is a non-generative

world model. We show that via architectural inductive biases, JEPAs can be leveraged to resolve the invariance-equivariance trade-off in SSL and enable processing of sequential action-observation pairs that is required to solve specific perception tasks. Unlike the majority of equivariant SSL methods discussed above, seq-JEPA does not use an equivariance predictor or loss function, nor does it require two pairs of views to which the same transformation is applied. We further highlight the differences between our framework and a recent equivariant method, ContextSSL. Specifically, seq-JEPA can be distinguished from ContextSSL on two aspects. First, unlike seq-JEPA, ContextSSL operates within the two-view SSL paradigm but uses a decoder-only transformer instead of the usual MLP projector so that its output embeddings are conditioned on the past. Second, while ContextSSL’s main goal is adapting equivariance to different transformations by alternating transformations in training data, our goal is to learn separate invariant and equivariant representations with respect to one or more transformations specified, and solve downstream tasks that require aggregating a sequence of action-observation pairs.

4. Experimental Setup

4.1. Compared methods and baselines

We compare seq-JEPA’s performance with both invariant and equivariant SSL methods. For invariant methods, we compare with SimCLR (Chen et al., 2020), BYOL (Grill et al., 2020), and VICReg (Bardes et al., 2022). For equivariant methods, we compare with SEN (Park et al., 2022), EquiMod (Devillers & Lefort, 2022), SIE (Garrido et al., 2023), and ContextSSL (Gupta et al., 2024). Additionally, we consider another equivariant baseline which we call Conditional BYOL, where BYOL’s predictor is conditioned on the action that transforms the view of the target branch to the view of the online branch, with the aim that transformation information is also encoded in representations. This architecture is equivalent to a two-view version of seq-JEPA with a sequence length of one during both training and inference, and with no sequence aggregator on top of representations. Furthermore, as a baseline for predictive learning across saccades, we consider a model which we call Conv-JEPA. This baseline has the same architecture as Conditional BYOL, and to train it, we consider the same sequence of patches that seq-JEPA uses (sampled from image saliencies), predict the representation of the last patch from each individual patch in the sequence, and sum their prediction losses. For architectural details of each baseline, see Section A.3.

4.2. Training protocol

For all methods, we use a ResNet-18 (He et al., 2016) (not pretrained) as the backbone encoder. For experiments that

use CIFAR100 and low-resolution STL-10 patches in predictive learning across saccades, we use the CIFAR variant of ResNet-18. For action conditioning, similar to EquiMod (Devillers & Lefort, 2022), we use a learnable linear projection to learn action embeddings. In our default setting for all experiments with action conditioning, the action projector is 128-dimensional. For the sequence aggregator, we use a small transformer encoder (Vaswani et al., 2017) with three layers, four attention heads, and post-normalization. For the predictor, we use an MLP with a hidden layer of 1024 dimensions and ReLU activation. In baseline comparisons, in order to control for and eliminate any performance gain resulting from using a transformer encoder in seq-JEPA instead of an MLP projection head, we train two variants of baselines that typically employ an MLP projector: one maintaining the original MLP projector and another where the projector is replaced with our transformer encoder. We report the higher performance among the two models. For a fair comparison, all models are trained for a fixed batch size of 512 and the same number of epochs. For 3DIEBench experiments, all models are trained for 1000 epochs, while for other datasets, they are trained for 2000 epochs. For models that use a transformer as projector, including seq-JEPA, we use the AdamW optimizer with default β_1 and β_2 , a weight decay of 0.001, and a learning rate of 4×10^{-4} with a linear warmup for 20 epochs starting from 10^{-5} followed by a cosine decay back to 10^{-5} . For models that use an MLP projector, we use the Adam optimizer with a learning rate of 10^{-3} , default β_1 and β_2 , and no weight decay.

4.3. Evaluation metrics and protocol

To measure equivariance with respect to a specific transformation, we perform action decoding from encoder representations as in Garrido et al. (2023). Specifically, given two transformed views, we extract representations from the frozen encoder, concatenate them, and train a regression head on top to predict the relative transformation (action) between the two. We report the R^2 score of this regressor on the test set as the equivariance metric. Although not always a perfect measure of invariance (Wang et al., 2024), we report top-1 classification accuracy of a linear probe as an approximate metric for representational invariance. For all baselines, we report the accuracy based on encoder representations. For seq-JEPA, we measure accuracies on top of the aggregate representation (z_{AGG} in Figure 2). When reporting accuracy based on z_{AGG} , we report the number of observation views (context lengths) used during both training and inference. For completeness, we also report classification performance on top of encoder representation (z_i in Figure 2) for all seq-JEPA models in Section B.4. Details on training the evaluation probes are given in Section A.2.

5. Results

5.1. Quantitative evaluation on 3DIEBench

We use the 3DIEBench benchmark to quantitatively compare invariant and equivariant representations in seq-JEPA with baseline methods. This benchmark allows us to measure equivariance through decoding 3D object rotations while enabling invariance measurement through object category classification. Table 1 provides a summary of our evaluation results on the 3DIEBench dataset where equivariant methods have been conditioned on rotation. In addition to the relative rotation between two views, in the last column, we provide the R^2 score for predicting individual transformation parameters from representations of a single view. For seq-JEPA, we trained models with training sequence lengths between one to four (denoted by M_{tr} in the table) and measure the linear classification performance with different inference lengths (denoted by M_{val}) on top of the aggregate representation. Among the invariant methods, BYOL achieves the highest classification accuracy, yet does not offer a high level of equivariance. Among equivariant baselines, while EquiMod and SEN offer even better classification accuracy compared to invariant methods, in terms of equivariance, they lag behind SIE and ContextSSL which provide the best rotation prediction performance due to their specialized equivariance predictors and loss functions. Even though both SIE and ContextSSL representations become highly sensitive to rotation, they do not fare well in linear probe classification. Seq-JEPA is able to achieve a rotation R^2 on a par with the best performing equivariant method while outperforming all methods in classification thanks to sequence aggregation during training and inference with a margin that increases with the inference sequence length. Finally, when action conditioning is ablated (last row in the table), seq-JEPA loses its equivariant properties, yet maintains a strong classification performance. For additional results on 3DIEBench including models with different training and inference sequence lengths and models conditioned on rotation and color, see Sections B.1 to B.3.

5.2. Qualitative evaluation on 3DIEBench

In order to qualitatively evaluate the representations learned by seq-JEPA and shed some light on its invariance-equivariance properties, we conduct two different visualizations. First, to see equivariance in representational space, we retrieve the three nearest representations of a query image from the validation set of 3DIEBench (Figure 4). All methods successfully retrieve the correct object category, while only seq-JEPA and SIE, which demonstrate high quantitative equivariance performance (Table 1), maintain rotation equivariance across all three nearest representations.

In the second visualization, we plot the 2D UMAP projections of seq-JEPA’s encoder and aggregate representations

Table 1: Quantitative evaluation of learned representations on 3DIEBench for rotation prediction (equivariance) and linear probe classification (invariance). Equivariant models and seq-JEPA are conditioned on rotation. For seq-JEPA, the training sequence length is denoted by M_{tr} and probing on top of z_{AGG} is done with an inference length M_{val} .

Method	Classification (top-1)	Relative Rotation (R^2)	Individual Rotation (R^2)
Invariant			
BYOL	82.90	0.12	0.25
SimCLR	81.13	0.35	0.54
VICReg	80.48	0.20	0.36
Equivariant			
SEN	83.43	0.35	0.57
EquiMod	84.29	0.32	0.55
SIE	77.49	0.58	0.62
Conditional BYOL	82.61	0.31	0.47
ContextSSL ($c = 126$)	80.4	0.74	0.78
Invariant-Equivariant			
seq-JEPA ($M_{tr} = 1, M_{val} = 1$)	84.08	0.65	0.69
seq-JEPA ($M_{tr} = 1, M_{val} = 3$)	85.31	0.65	0.69
seq-JEPA ($M_{tr} = 3, M_{val} = 3$)	86.14	0.71	0.74
seq-JEPA ($M_{tr} = 3, M_{val} = 5$)	87.41	0.71	0.74
seq-JEPA (w/o act cond, $M_{tr, val} = 3$)	86.05	0.29	0.37

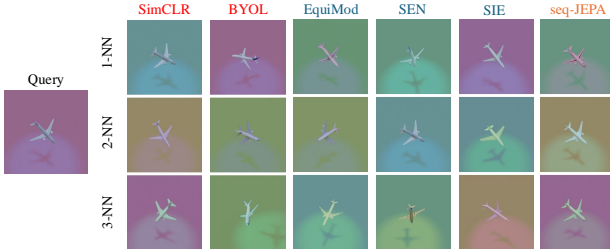


Figure 4: Retrieval of nearest representations; given a query image, we extract the three nearest encoder representations in the validation set of 3DIEBench. The retrieved views of models with the highest quantitative rotation equivariance performance maintain the rotation of the query image.

(Figure 5) for the model trained conditioned on rotation. The left panel of Figure 5 shows encoder representations colored by class label, while the middle panel displays the same encoder representations colored by rotation angle. The smooth color gradation across the map within each class cluster in this middle panel suggests that the encoder captures rotation angle as a continuous factor, implying equivariance to rotation (e.g., the red class in the bottom-right corner of the right panel and the corresponding part in the middle panel). The right panel shows aggregate representations colored by class label. Comparing the class-colored plots (left and right panels), we observe that both encoder and aggregate representations contain class information. However, when we aggregate multiple views of a sample, some of the intra-class variability (resulting from transformations such as rotation) is eliminated, causing each class's representational cluster to become more homogeneous.

This aggregation procedure likely reduces variation due to rotation and makes the representations more invariant, resulting in decreased intra-class spread and increased inter-class distance. We create a similar UMAP visualization for seq-JEPA with ablated rotation conditioning in Section B.5 which highlights the role of action conditioning in achieving equivariance to rotation.

5.3. Evaluation of models trained using hand-crafted augmentations

We next quantitatively assess invariance and equivariance for the second set of transformations, i.e. hand-crafted augmentations. Table 2 provides a summary of our evaluation on models trained on CIFAR100 and Tiny ImageNet. For each equivariant method and seq-JEPA, we trained four different variations. In three variations, the model is conditioned on only one of the augmentations among cropping, color jittering, and blurring, and in the last variation, on all three augmentations. Considering equivariance to augmentations, seq-JEPA outperforms invariant and equivariant baselines by a large margin. Notably, except for the model trained on CIFAR-100 and conditioned on blur, the best equivariance performance for a given augmentation is achieved when the model is specialized and conditioned only on that augmentation. Furthermore, ablating actions (last row in the table) causes seq-JEPA to achieve a lower equivariance performance across transformations compared to action-conditioned models. In terms of linear probe classification accuracy on top of aggregate representations, our framework is competitive with both invariant and equivariant families, yet does not outperform all of them. For

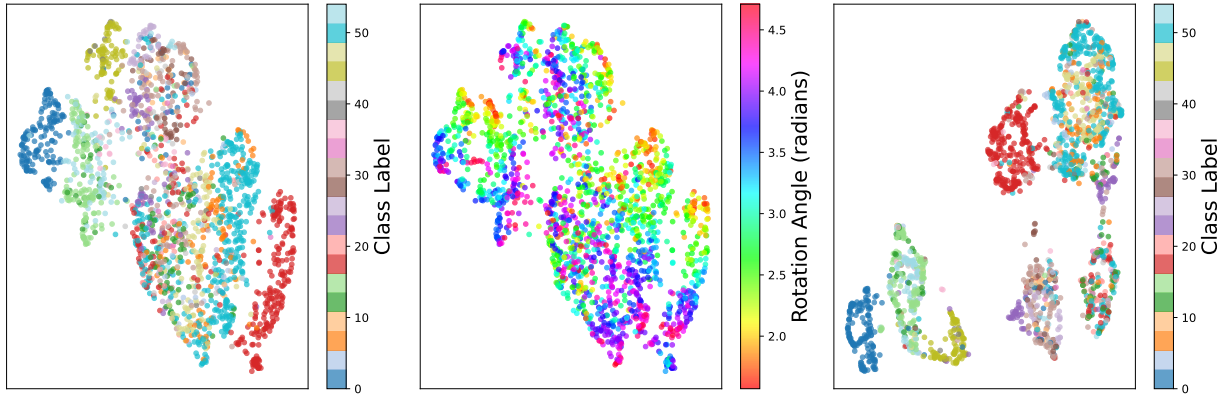


Figure 5: Visualization of 2-D UMAP projections of seq-JEPA’s encoder and aggregate representations. The model is trained on 3DIEBench and conditioned on rotation with $M_{tr} = 3$ and $M_{val} = 5$. Encoder representations for each view observation, color-coded by class category (**left**) and rotation angle (**middle**). The aggregate token representation for $M_{val} = 5$ observations during inference, color-coded by class category (**right**).

additional results with different training and inference sequence lengths for seq-JEPA models trained with augmented views, see Section B.3.

5.4. Predictive learning across saccades

Quantitative evaluation. In our third action-observation setting, we consider predictive learning across simulated eye movements to exhibit seq-JEPA’s ability in leveraging a sequence of partial observations alongside actions to learn visual representations. Table 3 summarizes our evaluation results for predictive learning across saccades on STL-10. While seq-JEPA only uses low-resolution patches with no augmentation, it achieves a classification performance comparable to SimCLR, an invariant model that is trained using strongly augmented image views with full resolution. Ablating action conditioning causes the accuracy on top of the aggregate representations to drop significantly, indicating that positional awareness is essential to forming semantic representations across simulated eye movements. Furthermore, comparison with the Conv-JEPA baseline highlights the importance of aggregating a sequence of patch representations in contrast to simply accumulating prediction errors between pairs of patches. Additionally, the last two ablation results in the table show that saliency-driven sampling of patches alongside IoR play a key role in sampling informative and non-overlapping patches and achieving high-quality aggregate representations. Interestingly, while random uniform patch sampling negatively impacts classification accuracy, it results in the highest positional equivariance, as the model samples patches and corresponding saccade actions from across the entire image and not just the salient regions.

Qualitative evaluation. Figure 6 shows UMAP projections for seq-JEPA representations trained on STL-10 via predictive learning across saccades. As for rotation in Figure 5,

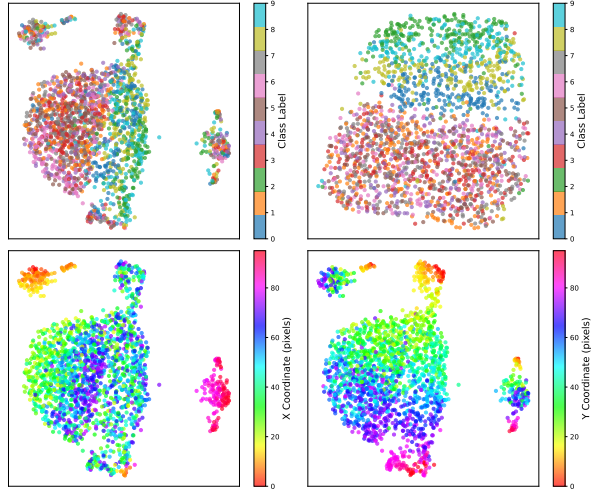


Figure 6: Visualization of 2-D UMAP projections of seq-JEPA’s encoder and aggregate representations. The model is trained on STL-10 via predictive learning across saccades and conditioned on fixation position with $M_{tr, val} = 4$. Encoder representations for each view observation, color-coded by class category (**top-left**) and X and Y pixel coordinates (**bottom** panels). The aggregate token representation for $M_{val} = 4$ observation patches during inference, color-coded by class category (**top-right**).

equivariance to fixation position can be observed from the bottom panels that show UMAP projection of encoder representations color-coded by X and Y coordinates. Similar to rotation in 3DIEBench, we provide a similar UMAP visualization for seq-JEPA with ablated position conditioning in Section B.5 for predictive learning across saccades to highlight the role of action conditioning.

Table 2: Quantitative evaluation of learned representations with hand-crafted augmentations on CIFAR100 and Tiny ImageNet; equivariance is measured by predicting relative transformation parameters associated with crop, color jitter, or blur augmentations. For seq-JEPA, the training sequence length is denoted by M_{tr} and probing is done with an inference length (M_{val}) of five.

Conditioning	Method	CIFAR100				Tiny ImageNet			
		Classification (top-1)	Crop (R^2)	Jitter (R^2)	Blur (R^2)	Classification (top-1)	Crop (R^2)	Jitter (R^2)	Blur (R^2)
Invariant									
-	SimCLR	61.72	0.56	0.18	0.04	34.29	0.30	0.08	0.13
	BYOL	62.17	0.39	0.05	-0.01	35.70	0.17	0.01	0.16
	VICReg	61.35	0.49	0.11	-0.06	35.29	0.31	0.05	0.19
Equivariant									
Crop+Jitter+Blur	SEN	61.94	0.65	0.51	0.85	36.01	0.24	0.48	0.87
	EquiMod	61.80	0.59	0.49	0.74	36.75	0.38	0.46	0.86
	SIE	58.81	0.34	0.26	0.53	31.37	0.26	0.56	0.88
	Conditional BYOL	60.63	0.56	0.46	0.73	35.49	0.34	0.54	0.87
Crop	SEN	61.56	0.66	0.15	0.10	35.95	0.24	0.11	0.49
	EquiMod	61.77	0.62	0.15	0.01	36.83	0.26	0.12	0.30
	SIE	57.55	0.69	0.11	0.25	32.38	0.34	0.05	0.14
	Conditional BYOL	60.17	0.55	0.10	-0.01	37.07	0.22	0.01	0.24
Color jitter	SEN	61.78	0.50	0.52	0.02	36.59	0.26	0.50	0.21
	EquiMod	61.53	0.44	0.50	-0.02	37.18	0.20	0.52	0.29
	SIE	59.29	0.48	0.59	0.06	34.37	0.39	0.62	0.35
	Conditional BYOL	61.30	0.36	0.52	0.02	37.93	0.24	0.62	0.30
Blur	SEN	61.47	0.43	0.15	0.84	34.62	0.16	0.08	0.79
	EquiMod	62.72	0.41	0.15	0.74	36.12	0.24	0.10	0.91
	SIE	57.66	0.40	0.07	0.71	31.00	0.26	0.05	0.85
	Conditional BYOL	60.74	0.36	0.11	0.69	36.17	0.19	0.02	0.85
Invariant-Equivariant									
Crop+Jitter+Blur	seq-JEPA ($M_{tr} = 1$)	52.90	0.77	0.52	0.23	37.10	0.64	0.49	0.89
	seq-JEPA ($M_{tr} = 2$)	60.17	0.78	0.64	0.88	35.56	0.69	0.42	0.93
	seq-JEPA ($M_{tr} = 3$)	58.33	0.79	0.63	0.92	34.85	0.67	0.64	0.96
Crop	seq-JEPA ($M_{tr} = 2$)	59.32	0.78	0.01	0.10	35.74	0.70	0.12	0.46
	seq-JEPA ($M_{tr} = 3$)	58.62	0.68	0.68	0.29	35.21	0.60	0.66	0.62
Color Jitter	seq-JEPA ($M_{tr} = 3$)	56.82	0.71	0.15	0.74	35.79	0.58	0.22	0.97
	seq-JEPA ($M_{tr} = 2$)	58.37	0.64	0.14	0.16	35.97	0.52	0.18	0.47

Table 3: Quantitative evaluation of predictive learning across saccades on STL-10. Equivariance is measured with respect to the position of a fixated patch on the image. Seq-JEPA models use only low-resolution patches with no augmentation during training and inference. Unless stated otherwise, training and inference lengths (M_{tr} and M_{val}) are set to four for all seq-JEPA variants.

Conditioning	Classification (top-1)	Position (R^2)
Invariant		
-	SimCLR (augmentations)	85.23
Equivariant		
position	Conv-JEPA ($M_{tr, val} = 4$)	80.04
Invariant-Equivariant		
position	seq-JEPA	70.45
	seq-JEPA	83.44
position	seq-JEPA ($M_{val} = 6$)	84.12
position	seq-JEPA (no saliency)	79.85
position	seq-JEPA (no IoR)	77.97

5.5. Path integration across actions

While an agent executes a sequence of actions in an environment, transitioning from an initial state to a final state, it should be capable of tracking its position by integrating its own actions. This is also a crucial cognitive ability that enables animals to estimate their current state in their habitat (McNaughton et al., 2006). Here, we evaluate whether pre-trained seq-JEPA is able to solve *path integration*. Given the sequence of observations $\{x_i\}_{i=1}^{M+1}$ generated from transformations $\{t_i\}_{i=1}^{M+1}$ and the corresponding action embeddings $\{a_i\}_{i=1}^M$, we define the task of path integration over the se-

quence of actions as predicting the relative action that would directly transform x_1 to x_{M+1} (which we denote as $a_{1,M}$) given z_{AGG} and a_M . In other words, given the aggregate representation of a sequence of action-observation pairs and the next action, we would like to predict the overall position change from the starting point (x_1) to the end point (x_{M+1}). We consider path integration for rotation angles in 3DIEBench and across eye movements with STL-10. For rotations, the task is integrating a series of object rotations from the first view to the last, i.e. angular path integration. For eye movements, the task is integrating the eye movements from the first saccade to the last, i.e. visual path integration. To measure path integration performance, we train a regression head on top of the concatenation of z_{AGG} and a_M to predict $a_{1,M}$ for a given inference sequence length. Figure 7 shows the results for both angular and visual path integration. The red curve corresponds to the performance of the original seq-JEPA. The blue curve corresponds to experiments in which the action embeddings are ablated (they are set to zero during inference for all views). The green curve corresponds to experiments in which the encoder (visual) representations are ablated (they are set to zero when being concatenated with actions before being fed to the transformer). As expected, path integration becomes more difficult as the number of observations increases (red curves). Ablating action conditioning (blue curves) results in failure of path integration. On the other hand, ablating the visual representations (green curves) results only in a

small performance drop compared to the original model, indicating that action conditioning is the key factor enabling path integration.

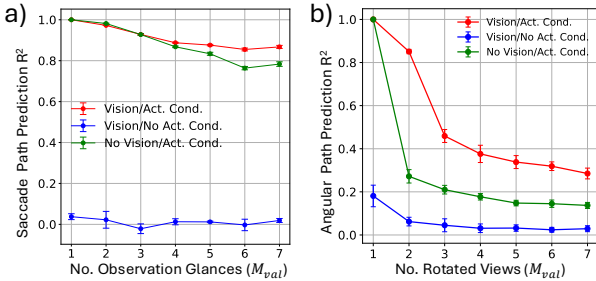


Figure 7: a) Visual path integration across eye movements, b) Angular path integration across object rotations (results over three random seeds)

5.6. Role of action conditioning

To better understand the importance of action conditioning in learning highly equivariant representations, we perform ablation experiments for seq-JEPA trained on 3DIEBench by changing the dimensionality of action embeddings and ablating actions from one of the two or both components of seq-JEPA, i.e. the transformer encoder and the MLP predictor. These ablation results are provided in Table 4. An important observation is that both predictor and transformer action conditioning are important in achieving the best equivariant performance, yet predictor action conditioning plays a more important role. Furthermore, learnable action embeddings play a key role in developing equivariance to rotation, although this equivariance shows little sensitivity to the dimensionality of the action embedding. Additionally, classification performance is slightly boosted in the presence of action conditioning, yet its role in this case is not as important compared to positional embeddings in predictive learning across saccades.

5.7. Role of training and inference sequence lengths

In order to study the effect of training and inference sequence lengths on our framework’s performance, we trained seq-JEPA with different training sequence lengths and measured both equivariance of encoder representations and linear probe accuracy using different inference sequence lengths to form the aggregate representation (Figure 8). A general positive trend can be observed in equivariance performance for different transformations when increasing the training sequence length (Figure 8, left panel), which can be the impact of seeing more action-conditioned representations during training. For linear classification (invariance-related performance; Figure 8, middle panel), the models trained on 3DIEBench and via predictive learning across saccades benefit from a longer training sequence length.

Table 4: Ablation results on the effect of seq-JEPA’s action conditioning trained on 3DIEBench (equivariance to rotation); we investigate the effects of partial or complete action ablations and changing the dimensionality of action embeddings on linear classification and rotation prediction performance. All models have $M_{tr} = 3$ and $M_{val} = 5$ and results are reported over three random seeds.

Variant	Classification (top-1)	Rotation (R^2)
Act. conditioning		
None	87.36 ± 0.7	0.29 ± 0.04
Random noise	58.16 ± 3.2	0.20 ± 0.07
Ablated predictor act cond.	87.17 ± 0.3	0.37 ± 0.06
Ablated transformer act cond.	86.33 ± 0.1	0.53 ± 0.05
Act. embedding dim		
Non-learnable act emb	85.68 ± 0.2	0.34 ± 0.04
<i>adim</i> = 16	86.29 ± 0.4	0.70 ± 0.01
<i>adim</i> = 64	87.11 ± 0.2	0.70 ± 0.02
<i>adim</i> = 128 (default)	87.41 ± 0.5	0.71 ± 0.02
<i>adim</i> = 256	87.26 ± 0.6	0.72 ± 0.00

However, in the augmentation setting with CIFAR100, a small drop in accuracy is observed for higher training sequence lengths. The observed differences across evaluation tasks likely stem from specific task requirements. We hypothesize that leveraging and aggregating a sequence of action-observation pairs, i.e. seq-JEPA’s architectural inductive bias, is most effective in settings where the downstream task benefits from sequential observation. In the case of object rotations in 3DIEBench, seeing an object from multiple angles is indeed beneficial in recognizing the object’s category, which explains the improved classification accuracy with increased sequence length. Similarly, in the case of predictive learning across saccades, each eye movement and its subsequent glance provides additional information that can be leveraged for learning a richer aggregate representation. Such an advantage may not be present when using artificially-augmented images which can also explain the classification performance gap between seq-JEPA and the best-performing baselines in this setting (Table 2). Finally, during inference (Figure 8, right panel), all transformation settings benefit from more views and a richer context to improve the quality of aggregate representation.

6. Limitations and Future Perspectives

In this paper, we proposed seq-JEPA, a world modeling paradigm for learning architecturally segregated transformation-invariant and -equivariant representations. Although we have shown the feasibility of our world model for multiple transformation settings in image modality, we have not yet explored other modalities such as video, text, or multi-modal data. Given the architecture of seq-JEPA, it is possible to utilize the sequence aggregator to fuse representations from multiple modalities. Another promising direction is to build efficient world models for embodied

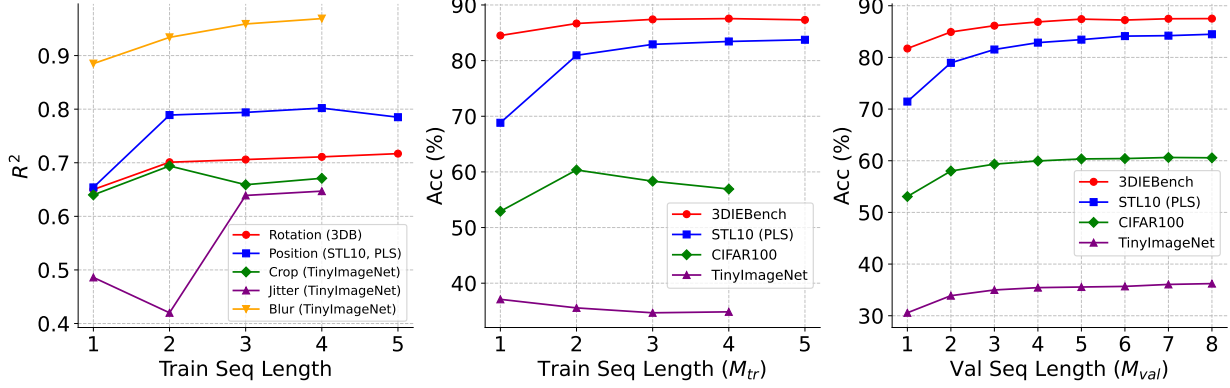


Figure 8: Effect of training and inference sequence length on seq-JEPA’s performance; **left:** Equivariant performance (R^2) for different training sequence lengths (inference sequence length fixed); **middle:** Classification performance on top of aggregate representations versus training sequence length (inference sequence length fixed); **right:** Classification performance on top of aggregate representations for different inference sequence lengths (training sequence length fixed)

agents with egocentric vision via scaling our approach to larger image and video datasets and take advantage of a sequence of *foveated* observations based on salience in a setup similar to predictive learning across saccades. Our transfer learning results on ImageNet-1k in Section B.6 hints at the possibility of building such a world model. Finally, similar to other equivariant SSL techniques, seq-JEPA requires knowledge of transformation groups. Developing a group-agnostic equivariant method is a challenge that remains largely unexplored in SSL.

Acknowledgements

This project was supported by funding from NSERC (Discovery Grants RGPIN-2022-05033 to E.B.M., and RGPIN-2023-03875 to S.B.), Canada CIFAR AI Chairs Program and Google to E.B.M., Canada Excellence Research Chairs (CERC) Program, Mila - Quebec AI Institute, Institute for Data Valorization (IVADO), CHU Sainte-Justine Research Centre, Fonds de Recherche du Québec-Santé (FRQS), and a Canada Foundation for Innovation John R. Evans Leaders Fund grant to E.B.M. This research was also supported in part by Digital Research Alliance of Canada (DRAC) and Calcul Québec.

References

Assran, M., Caron, M., Misra, I., Bojanowski, P., Bordes, F., Vincent, P., Joulin, A., Rabbat, M., and Ballas, N. Masked Siamese Networks for Label-Efficient Learning. In *Proceedings of the 17th European Conference on Computer Vision, ECCV 2022*, April 2022. URL <http://arxiv.org/abs/2204.07141>. arXiv:2204.07141 [cs, eess].

Assran, M., Duval, Q., Misra, I., Bojanowski, P., Vincent, P., and Ballas, N. Self-Supervised Learning from Images with a Joint-Embedding Predictive Architecture. In *2023 IEEE/CVF Conference on Computer Vision and Pattern Recognition (CVPR)*, pp. 15619–15629, Vancouver, BC, Canada, June 2023. IEEE. ISBN 979-8-3503-0129-8. doi: 10.1109/CVPR52729.2023.01499. URL <https://ieeexplore.ieee.org/document/10205476/>.

Baevski, A., Hsu, W.-N., Xu, Q., Babu, A., Gu, J., and Auli, M. data2vec: A General Framework for Self-supervised Learning in Speech, Vision and Language. In *Proceedings of the 39th International Conference on Machine Learning*, pp. 1298–1312. PMLR, June 2022. URL <https://proceedings.mlr.press/v162/baevski22a.html>. ISSN: 2640-3498.

Bao, H., Dong, L., Piao, S., and Wei, F. BEiT: BERT Pre-Training of Image Transformers. In *International Conference on Learning Representations*, October 2021. URL <https://openreview.net/forum?id=p-BhZSz59o4>.

Bardes, A., Ponce, J., and LeCun, Y. VICReg: Variance-Invariance-Covariance Regularization for Self-Supervised Learning. In *International Conference on Learning Representations*, 2022. URL <https://openreview.net/forum?id=xm6YD62D1Ub>.

Caron, M., Misra, I., Mairal, J., Goyal, P., Bojanowski, P., and Joulin, A. Unsupervised Learning of Visual Features by Contrasting Cluster Assignments. In *Advances in Neural Information Processing Systems*, volume 33, pp. 9912–9924. Curran Associates, Inc., 2020.

Caron, M., Touvron, H., Misra, I., Jégou, H., Mairal, J., Bojanowski, P., and Joulin, A. Emerging Properties in Self-Supervised Vision Transformers. In

Proceedings of the IEEE/CVF International Conference on Computer Vision, pp. 9650–9660, 2021.
URL https://openaccess.thecvf.com/content/ICCV2021/html/Caron_Emerging_Properties_in_Self-Supervised_Vision_Transformers_ICCV_2021_paper.html.

Chen, T., Kornblith, S., Norouzi, M., and Hinton, G. A Simple Framework for Contrastive Learning of Visual Representations. In *Proceedings of the 37th International Conference on Machine Learning*, pp. 1597–1607. PMLR, November 2020. URL <https://proceedings.mlr.press/v119/chen20j.html>. ISSN: 2640-3498.

Chen, X. and He, K. Exploring Simple Siamese Representation Learning. In *Proceedings of the IEEE/CVF Conference on Computer Vision and Pattern Recognition*, pp. 15750–15758, 2021. URL https://openaccess.thecvf.com/content/CVPR2021/html/Chen_Exploring_Simple_Siamese_Representation_Learning_CVPR_2021_paper.html.

Dangovski, R., Jing, L., Loh, C., Han, S., Srivastava, A., Cheung, B., Agrawal, P., and Soljacic, M. Equivariant Self-Supervised Learning: Encouraging Equivariance in Representations. In *International Conference on Learning Representations*, 2022. URL <https://openreview.net/forum?id=gKLAIfiytI>.

Dawid, A. and LeCun, Y. Introduction to latent variable energy-based models: a path toward autonomous machine intelligence. *Journal of Statistical Mechanics: Theory and Experiment*, 2024(10):104011, October 2024. ISSN 1742-5468. doi: 10.1088/1742-5468/ad292b. URL <https://dx.doi.org/10.1088/1742-5468/ad292b>. Publisher: IOP Publishing.

Devillers, A. and Lefort, M. EquiMod: An Equivariance Module to Improve Visual Instance Discrimination. In *The Eleventh International Conference on Learning Representations*, September 2022. URL <https://openreview.net/forum?id=eDLwjKmtYFt>.

Dosovitskiy, A., Beyer, L., Kolesnikov, A., Weissenborn, D., Zhai, X., Unterthiner, T., Dehghani, M., Minderer, M., Heigold, G., Gelly, S., Uszkoreit, J., and Houlsby, N. An Image is Worth 16x16 Words: Transformers for Image Recognition at Scale. In *International Conference on Learning Representations*, October 2020. URL <https://openreview.net/forum?id=YicbFdNTTy>.

Dwibedi, D., Aytar, Y., Tompson, J., Sermanet, P., and Zisserman, A. With a Little Help From My Friends: Nearest-Neighbor Contrastive Learning of Visual Representations. In *Proceedings of the IEEE/CVF International Conference on Computer Vision*, pp. 9588–9597, 2021.

Ermolov, A., Siarohin, A., Sangineto, E., and Sebe, N. Whitening for Self-Supervised Representation Learning. In *Proceedings of the 38th International Conference on Machine Learning*, pp. 3015–3024. PMLR, July 2021. URL <https://proceedings.mlr.press/v139/ermolov21a.html>. ISSN: 2640-3498.

Garrido, Q., Najman, L., and Lecun, Y. Self-supervised learning of Split Invariant Equivariant representations. In *Proceedings of the 40th International Conference on Machine Learning*, pp. 10975–10996. PMLR, July 2023. URL <https://proceedings.mlr.press/v202/garrido23b.html>. ISSN: 2640-3498.

Garrido, Q., Assran, M., Ballas, N., Bardes, A., Najman, L., and LeCun, Y. Learning and Leveraging World Models in Visual Representation Learning, March 2024. URL <http://arxiv.org/abs/2403.00504>. arXiv:2403.00504 [cs].

Garrido, Q., Ballas, N., Assran, M., Bardes, A., Najman, L., Rabbat, M., Dupoux, E., and LeCun, Y. Intuitive physics understanding emerges from self-supervised pretraining on natural videos, February 2025. URL <http://arxiv.org/abs/2502.11831>. arXiv:2502.11831 [cs].

Gidaris, S., Singh, P., and Komodakis, N. Unsupervised Representation Learning by Predicting Image Rotations. February 2018. URL <https://openreview.net/forum?id=S1v4N210->.

Grill, J.-B., Strub, F., Altché, F., Tallec, C., Richemond, P., Buchatskaya, E., Doersch, C., Avila Pires, B., Guo, Z., Gheshlaghi Azar, M., Piot, B., kavukcuoglu, k., Munos, R., and Valko, M. Bootstrap Your Own Latent - A New Approach to Self-Supervised Learning. In *Advances in Neural Information Processing Systems*, volume 33, pp. 21271–21284. Curran Associates, Inc., 2020.

Guo, Z., Thakoor, S., Pislar, M., Avila Pires, B., Altché, F., Tallec, C., Saade, A., Calandriello, D., Grill, J.-B., Tang, Y., Valko, M., Munos, R., Gheshlaghi Azar, M., and Piot, B. BYOL-Explore: Exploration by Bootstrapped Prediction. In *Advances in Neural Information Processing Systems*, volume 35, pp. 31855–31870, December 2022.

Gupta, S., Robinson, J., Lim, D., Villar, S., and Jegelka, S. Structuring Representation Geometry with Rotationally Equivariant Contrastive Learning. In *The Twelfth International Conference on Learning Representations*, October 2023. URL <https://openreview.net/forum?id=lgaFMvZHSJ>.

Gupta, S., Wang, C., Wang, Y., Jaakkola, T., and Jegelka, S. In-Context Symmetries: Self-Supervised Learning through Contextual World Models. In *The Thirty-eighth Annual Conference on Neural Information Processing Systems*, November 2024. URL <https://openreview.net/forum?id=etPAH4xSU>.

Ha, D. and Schmidhuber, J. Recurrent World Models Facilitate Policy Evolution. In *Advances in Neural Information Processing Systems*, volume 31. Curran Associates, Inc., 2018. URL https://proceedings.neurips.cc/paper_files/paper/2018/hash/2de5d16682c3c35007e4e92982f1a2ba-Abstract.html.

Hafner, D., Lillicrap, T., Ba, J., and Norouzi, M. Dream to Control: Learning Behaviors by Latent Imagination. In *International Conference on Learning Representations*, September 2019. URL <https://openreview.net/forum?id=S11OTC4tDS>.

HaoChen, J. Z., Wei, C., Gaidon, A., and Ma, T. Provable Guarantees for Self-Supervised Deep Learning with Spectral Contrastive Loss. In *Advances in Neural Information Processing Systems*, volume 34, pp. 5000–5011. Curran Associates, Inc., 2021.

Harman, K. L., Humphrey, G., and Goodale, M. A. Active manual control of object views facilitates visual recognition. *Current Biology*, 9(22):1315–1318, November 1999. ISSN 09609822. doi: 10.1016/S0960-9822(00)80053-6. URL <https://linkinghub.elsevier.com/retrieve/pii/S0960982200800536>.

He, K., Zhang, X., Ren, S., and Sun, J. Deep Residual Learning for Image Recognition. In *2016 IEEE Conference on Computer Vision and Pattern Recognition (CVPR)*, pp. 770–778, Las Vegas, NV, USA, June 2016. IEEE. ISBN 978-1-4673-8851-1. doi: 10.1109/CVPR.2016.90. URL <http://ieeexplore.ieee.org/document/7780459/>.

He, K., Fan, H., Wu, Y., Xie, S., and Girshick, R. Momentum Contrast for Unsupervised Visual Representation Learning. In *2020 IEEE/CVF Conference on Computer Vision and Pattern Recognition (CVPR)*, pp. 9726–9735, Seattle, WA, USA, June 2020. IEEE. ISBN 978-1-72817-168-5. doi: 10.1109/CVPR42600.2020.00975. URL <https://ieeexplore.ieee.org/document/9157636/>.

He, K., Chen, X., Xie, S., Li, Y., Dollár, P., and Girshick, R. Masked Autoencoders Are Scalable Vision Learners. In *Proceedings of the IEEE/CVF Conference on Computer Vision and Pattern Recognition*, pp. 16000–16009, 2022. URL https://openaccess.thecvf.com/content/CVPR2022/html/He_Masked_Autoencoders_Are_Scalable_Vision_Learners_CVPR_2022_paper.html.

Itti, L., Koch, C., and Niebur, E. A model of saliency-based visual attention for rapid scene analysis. *IEEE Transactions on Pattern Analysis and Machine Intelligence*, 20(11):1254–1259, November 1998. ISSN 1939-3539. doi: 10.1109/34730558. URL <https://ieeexplore.ieee.org/document/730558/?arnumber=730558>. Conference Name: IEEE Transactions on Pattern Analysis and Machine Intelligence.

Khetarpal, K., Guo, Z. D., Pires, B. A., Tang, Y., Lyle, C., Rowland, M., Heess, N., Borsa, D. L., Guez, A., and Dabney, W. A Unifying Framework for Action-Conditional Self-Predictive Reinforcement Learning. In *The 28th International Conference on Artificial Intelligence and Statistics*, February 2025. URL <https://openreview.net/forum?id=5DypCUsMg4>.

LeCun, Y. A Path Towards Autonomous Machine Intelligence Version 0.9.2, 2022-06-27, 2022. OpenReview.

Lee, H., Lee, K., Lee, K., Lee, H., and Shin, J. Improving Transferability of Representations via Augmentation-Aware Self-Supervision. In *Advances in Neural Information Processing Systems*, volume 34, pp. 17710–17722. Curran Associates, Inc., 2021.

Li, Z. A saliency map in primary visual cortex. *Trends in Cognitive Sciences*, 6(1):9–16, January 2002. ISSN 1364-6613, 1879-307X. doi: 10.1016/S1364-6613(00)01817-9. URL [https://www.cell.com/trends/cognitive-sciences/abstract/S1364-6613\(00\)01817-9](https://www.cell.com/trends/cognitive-sciences/abstract/S1364-6613(00)01817-9). Publisher: Elsevier.

Linardos, A., Kummerer, M., Press, O., and Bethge, M. DeepGaze IIE: Calibrated prediction in and out-of-domain for state-of-the-art saliency modeling. In *2021 IEEE/CVF International Conference on Computer Vision (ICCV)*, pp. 12899–12908, Montreal, QC, Canada, October 2021. IEEE. ISBN 978-1-6654-2812-5. doi: 10.1109/ICCV48922.2021.01268. URL <https://ieeexplore.ieee.org/document/9711473/>.

McNaughton, B. L., Battaglia, F. P., Jensen, O., Moser, E. I., and Moser, M.-B. Path integration and the neural basis of the 'cognitive map'. *Nature Reviews Neuroscience*, 7(8):663–678, August 2006. ISSN 1471-0048. doi: 10.1038/nrn1932. URL <https://www.nature.com/articles/nrn1932>. Publisher: Nature Publishing Group.

Misra, I. and van der Maaten, L. Self-Supervised Learning of Pretext-Invariant Representations. In *Proceedings*

of the IEEE/CVF Conference on Computer Vision and Pattern Recognition, pp. 6707–6717, 2020. URL https://openaccess.thecvf.com/content_CVPR_2020/html/Misra_Self-Supervised_Learning_of_Pretext-Invariant_Representations_CVPR_2020_paper.html.

Ni, T., Eysenbach, B., SeyedSalehi, E., Ma, M., Gehring, C., Mahajan, A., and Bacon, P.-L. Bridging State and History Representations: Understanding Self-Predictive RL. In *The Twelfth International Conference on Learning Representations*, 2024. URL <https://openreview.net/forum?id=ms0VgzSGF2>.

Park, J. Y., Biza, O., Zhao, L., Meent, J.-W. V. D., and Walters, R. Learning Symmetric Embeddings for Equivariant World Models. In *Proceedings of the 39th International Conference on Machine Learning*, pp. 17372–17389. PMLR, June 2022. URL <https://proceedings.mlr.press/v162/park22a.html>. ISSN: 2640-3498.

Posner, M. I., Rafal, R. D., Choate, L. S., and Vaughan, J. Inhibition of return: Neural basis and function. *Cognitive Neuropsychology*, 2(3): 211–228, August 1985. ISSN 0264-3294, 1464-0627. doi: 10.1080/02643298508252866. URL <http://www.tandfonline.com/doi/abs/10.1080/02643298508252866>.

Scherr, F., Guo, Q., and Moraitis, T. Self-Supervised Learning Through Efference Copies. In *Advances in Neural Information Processing Systems*, October 2022. URL <https://openreview.net/forum?id=DotEQCtY67g>.

Schwarzer, M., Anand, A., Goel, R., Hjelm, R. D., Courville, A., and Bachman, P. Data-Efficient Reinforcement Learning with Self-Predictive Representations. In *International Conference on Learning Representations*, 2021. URL https://openreview.net/forum?id=uCQfpZwRaUu&fbclid=IwAR3FMvlynXXYEMJaJzPkilx1wC9jjA3aBDC_moWxrI91hLaDvtk7nnnIXT8.

Shakerinava, M., Mondal, A. K., and Ravanbakhsh, S. Structuring Representations Using Group Invariants. In *Advances in Neural Information Processing Systems*, volume 35, pp. 34162–34174, December 2022.

Sobal, V., Zhang, W., Cho, K., Balestriero, R., Rudner, T. G. J., and LeCun, Y. Learning from Reward-Free Offline Data: A Case for Planning with Latent Dynamics Models, February 2025. URL <https://arxiv.org/abs/2502.14819>. arXiv:2502.14819 [cs].

Tang, Y., Guo, Z. D., Richemond, P. H., Pires, B. A., Chandak, Y., Munos, R., Rowland, M., Azar, M. G., Lan, C. L., Lyle, C., György, A., Thakoor, S., Dabney, W., Piot, B., Calandriello, D., and Valko, M. Understanding Self-Predictive Learning for Reinforcement Learning. In *Proceedings of the 40th International Conference on Machine Learning*, pp. 33632–33656. PMLR, July 2023. URL <https://proceedings.mlr.press/v202/tang23d.html>. ISSN: 2640-3498.

Tarr, M. J., Williams, P., Hayward, W. G., and Gauthier, I. Three-dimensional object recognition is viewpoint dependent. *Nature Neuroscience*, 1(4):275–277, August 1998. ISSN 1546-1726. doi: 10.1038/1089. URL https://www.nature.com/articles/nn0898_275. Publisher: Nature Publishing Group.

van den Oord, A., Li, Y., and Vinyals, O. Representation Learning with Contrastive Predictive Coding, January 2019. URL <https://arxiv.org/abs/1807.03748>. arXiv:1807.03748 [cs, stat].

Vaswani, A., Shazeer, N., Parmar, N., Uszkoreit, J., Jones, L., Gomez, A. N., Kaiser, L., and Polosukhin, I. Attention is All you Need. In *Advances in Neural Information Processing Systems*, volume 30. Curran Associates, Inc., 2017.

Vuilleumier, P., Henson, R. N., Driver, J., and Dolan, R. J. Multiple levels of visual object constancy revealed by event-related fMRI of repetition priming. *Nature Neuroscience*, 5(5):491–499, May 2002. ISSN 1546-1726. doi: 10.1038/nn839. URL <https://www.nature.com/articles/nn839>. Publisher: Nature Publishing Group.

Wang, Y., Hu, K., Gupta, S., Ye, Z., Wang, Y., and Jegelka, S. Understanding the Role of Equivariance in Self-supervised Learning. In *The Thirty-eighth Annual Conference on Neural Information Processing Systems*, November 2024. URL <https://openreview.net/forum?id=NLqdudgBfy>.

Xiao, T., Wang, X., Efros, A. A., and Darrell, T. What Should Not Be Contrastive in Contrastive Learning. In *International Conference on Learning Representations*, 2021. URL <https://openreview.net/forum?id=CZ8Y3NzuVzO>.

Xie, Z., Zhang, Z., Cao, Y., Lin, Y., Bao, J., Yao, Z., Dai, Q., and Hu, H. SimMIM: A Simple Framework for Masked Image Modeling. In *Proceedings of the IEEE/CVF Conference on Computer Vision and Pattern Recognition (CVPR)*, 2022, pp. 9653–9663, 2022.

Yeh, C.-H., Hong, C.-Y., Hsu, Y.-C., Liu, T.-L., Chen, Y., and LeCun, Y. Decoupled Contrastive Learning. In Avi- dan, S., Brostow, G., Cissé, M., Farinella, G. M., and Has- sner, T. (eds.), *Computer Vision – ECCV 2022*, pp. 668– 684, Cham, 2022. Springer Nature Switzerland. ISBN 978-3-031-19809-0. doi: 10.1007/978-3-031-19809-0- 38.

Yerxa, T. E., Feather, J., Simoncelli, E. P., and Chung, S. Contrastive-Equivariant Self-Supervised Learn- ing Improves Alignment with Primate Visual Area IT. November 2024. URL <https://openreview.net/forum?id=AiMs8GPP5q>.

Zbontar, J., Jing, L., Misra, I., LeCun, Y., and Deny, S. Bar- low Twins: Self-Supervised Learning via Redundancy Reduction. In *Proceedings of the 38th International Con- ference on Machine Learning*, pp. 12310–12320. PMLR, July 2021. URL <https://proceedings.mlr.press/v139/zbontar21a.html>. ISSN: 2640- 3498.

Zhaoping, L. The V1 hypothesis—creating a bottom- up saliency map for preattentive selection and seg- mentation. In *Understanding Vision*, pp. 189– 314. Oxford University PressOxford, 1 edition, May 2014. ISBN 978-0-19-956466-8 978-0-19-177250- 4. doi: 10.1093/acprof:oso/9780199564668.003. 0005. URL <https://academic.oup.com/book/8719/chapter/154784147>.

A. Implementation Details

A.1. Data preparation

3DIEBench. The original 256×256 images are resized to a 128×128 resolution for all experiments. Normalization is done using the means and standard deviations provided by [Garrido et al. \(2023\)](#), i.e., $\mu = [0.5016, 0.5037, 0.5060]$ and $\sigma = [0.1030, 0.0999, 0.0969]$ for the three RGB channels, respectively.

CIFAR100. We use 32×32 images with normalization parameters typically used in the literature, i.e., $\mu = [0.4914, 0.4822, 0.4465]$ and $\sigma = [0.247, 0.243, 0.261]$. For data augmentation, we follow EquiMod’s augmentation strategy.

Tiny ImageNet. The training set consists of 100000 ImageNet-1k images from 200 classes (500 for each class) downsized to 64×64 . The validation set has 50 images per class. We use normalization parameters $\mu = [0.4914, 0.4822, 0.4465]$ and $\sigma = [0.247, 0.243, 0.261]$, for the three RGB channels, respectively. For data augmentation, we use the same augmentation parameters as CIFAR100 with the kernel size of Gaussian blur adapted to the 64×64 images.

STL10. In order to extract the saliencies, we resize images to 512×512 , feed them to the pre-trained DeepGaze IIE ([Linardos et al., 2021](#)), resize the output saliencies back to 96×96 , and store them alongside original images. We use normalization parameters $\mu = [0.4467, 0.4398, 0.4066]$, $\sigma = [0.2241, 0.2215, 0.2239]$ for the three RGB channels, respectively. After sampling fixations from saliencies, the patches are extracted from the image to simulate foveation are 32×32 (compared to the full image size of 96×96).

Transformation parameters. For 3DIEBench, we use the rotation and color parameters provided with images for action conditioning as done in ([Garrido et al., 2023](#)). For the augmentation setting, we use the parameters corresponding to each of the three augmentations and form the action as the relative augmentation vector between two images. For crop, we use four variables, i.e., vertical and horizontal coordinate, and height and width. For color jitter, we use four variables: brightness, contrast, saturation, and hue. For blur, we use one variable: the standard deviation of the blurring kernel. In predictive learning across saccades, the action is a 2-d vector, i.e., the normalized relative (x, y) coordinate between two patches.

A.2. Training and evaluation details

Protocols for training evaluation heads. For linear probing, we follow a common SSL protocol and train a linear classifier on top of frozen representations with a batch size of 256 for 300 epochs using the Adam optimizer with default hyperparameters. For action prediction, we follow a similar protocol as SIE ([Garrido et al., 2023](#)). Specifically, for rotation, color jitter, and crop, we train an MLP regressor with a hidden dimension of 1024 and ReLU activation for 300 epochs. For color (in 3DIEBench), blur (in the augmentation setting), and position (in predictive learning across saccades), we use a linear regressor and train it for 50 epochs. For path integration experiments, the same regressor architectures as the equivariance evaluation heads are used, i.e., the MLP for angular path integration and the linear regressor for saccade path integration. All regression heads are trained using the Adam optimizer with default hyperparameters.

Hardware. Each experiment was run on a single NVIDIA A100 GPU with 40GB of accelerator RAM. A single run of seq-JEPA on 3DIEBench with a training sequence length of three takes around 15 hours.

A.3. Architectural details

Below, we describe the architectural details and hyperparameters specific to each baseline.

BYOL. We use a projection head with 2048-2048-2048 intermediate dimensions. The predictor has a hidden dimension of 512-d with ReLU activation. We use the same EMA setup outlined in the original paper ([Grill et al., 2020](#)), i.e., the EMA parameter τ starts from $\tau_{\text{base}} = 0.996$ and is increased following a cosine schedule.

SimCLR. We use a temperature parameter of $\tau = 0.5$ with a projection MLP with 2048-2048-2048 intermediate dimensions.

VICReg. We use $\lambda_{\text{inv}} = \lambda_V = 10$, $\lambda_C = 1$, and a projection head with 2048-2048-2048 intermediate dimensions.

Conditional BYOL. The architecture is the same as BYOL, except that the predictor also receives the normalized relative transformation parameters. We use a linear action projector of 128-d and the same EMA setup as BYOL.

SIE. For both invariant and equivariant projection heads, we use intermediate dimensions of 1024-1024-1024. For the loss coefficients, we use $\lambda_{\text{inv}} = \lambda_V = 10$, $\lambda_{\text{equi}} = 4.5$, and $\lambda_C = 1$. We use the hypernetwork architecture for all experiments.

SEN. We use a temperature parameter of $\tau = 0.5$ with a projection MLP with 2048-2048-2048 intermediate dimensions.

EquiMod. We use the version based on SimCLR (both invariant and equivariant losses are contrastive with $\tau = 0.1$ and have equal weights). The projection head has 1024-1024-128 intermediate dimensions. We use a linear action projector of 128-d.

ContextSSL. We use the pre-trained weights provided by the authors (trained for 1000 epochs) and follow their evaluation protocol on 3DIEBench.

seq-JEPA. For the sequence aggregator, we use a transformer encoder with three layers, four attention heads, and post-normalization. For the predictor, we use an MLP with a hidden layer of 1024-d and ReLU activation. The linear action projector in our default setting is 128-d. We use the same EMA setup as BYOL.

B. Additional Experimental Results

B.1. Evaluation results on 3DIEBench for models conditioned on rotation and color

We further provide evaluation results for seq-JEPA and equivariant baselines on 3DIEBench conditioned on both rotation and color transformations in Table 5. The results show that all methods suffer a drop in classification performance and become highly sensitive to color. Similar performance degradations have been previously observed with 3DIEBench (Garrido et al., 2023; Gupta et al., 2024), yet without a convincing explanation. One possible explanation in line with Principle II in Wang et al. (2024) is that in 3DIEBench, floor and light hue are fairly decoupled from class information (low class relevance). Therefore, forcing the encoder to encode color information would cause class information to be lost, resulting in degradation of classification accuracy.

Table 5: Quantitative evaluation of learned representations on 3DIEBench for rotation and color prediction (equivariance) and linear probe classification (invariance). All models are conditioned on both rotation and color.

Method	Classification (top-1)	Rotation pred. (R^2)	Color pred. (R^2)
SEN	82.17	0.29	0.96
EquiMod	82.58	0.27	0.95
Conditional BYOL	81.95	0.38	0.94
SIE	75.34	0.46	0.97
seq-JEPA ($M_{tr} = 4$, $M_{val} = 5$)	79.31	0.52	0.97

B.2. Measuring invariance of aggregate representations

In order to have a sense of invariance of the aggregate representation, we tried to predict the individual rotation parameters of each view for a seq-JEPA model with $M_{val} = 3$ trained on 3DIEBench and conditioned on rotation. To avoid leaking the rotation parameters to z_{AGG} during prediction, we zero out the action embeddings. The mean R^2 score obtained by predicting individual rotations of the three views using z_{AGG} is 0.141 ± 0.002 ; which indicates that the aggregate representation has not encoded rotation in any of the views.

B.3. Complete evaluation results for linear probing on top of aggregate representations

In this section, we provide our complete evaluation results for linear probing on top of seq-JEPA’s aggregate representations for three transformation sets with different training and inference sequence lengths. Figure 9 shows the top-1 accuracy on

3DIEBench models conditioned on rotation. Figure 10 shows top-1 accuracy on STL-10 for models trained via predictive learning across saccades. Figures 11 and 12 show top-1 accuracy on CIFAR100 and Tiny ImageNet, respectively, with different types of action conditioning (crop, color jitter, blur, or all three). We can see the general trends of Figure 8 discussed in Section 5.7 also in these heatmaps.

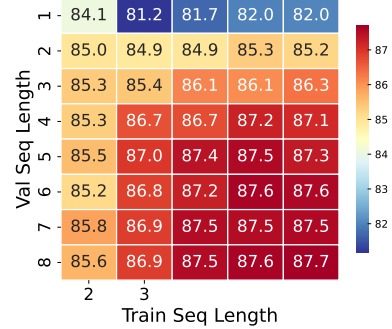


Figure 9: seq-JEPA’s performance on 3DIEBench with rotation conditioning; the heatmap shows linear probe accuracy on top of aggregate representations for different training and inference sequence lengths.



Figure 10: Seq-JEPA’s performance on STL-10 with predictive learning across saccades; the heatmap shows linear probe accuracy on top of aggregate representations for different training and inference sequence lengths.

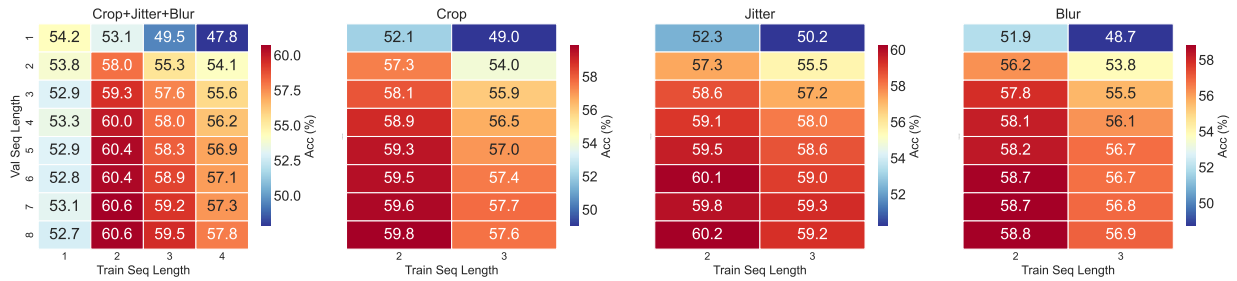


Figure 11: Seq-JEPA’s performance on CIFAR100 with different types of action conditioning (crop, color jitter, blur, or all three); the heatmap shows linear probe accuracy on top of aggregate representations for different training and inference sequence lengths.

B.4. Comparison of evaluation results on encoder representations and aggregate representations

For completeness, we provide linear probe classification on encoder representations for different transformation settings in Table 6 and compare them with accuracy on aggregate representations for different inference evaluation lengths. The aggregate representation generally achieves a higher classification performance thanks to the architectural inductive bias in seq-JEPA.

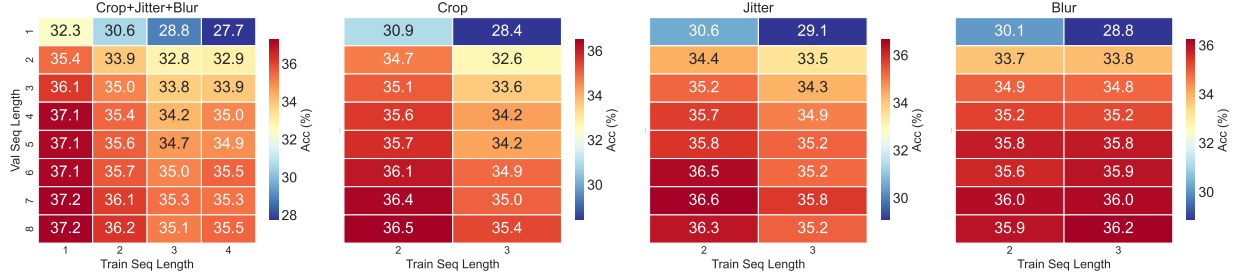


Figure 12: Seq-JEPA’s performance on Tiny ImageNet with different types of action conditioning (crop, color jitter, blur, or all three); the heatmap shows linear probe accuracy on top of aggregate representations for different training and inference sequence lengths.

Table 6: Comparison of seq-JEPA classification performance across datasets and conditioning. Top-1 classification accuracy is reported for z_{res} and z_{agg} , with varying inference lengths M_{eval} .

Dataset	Conditioning	M_{tr}	z_{res}	z_{agg}		
				$M_{eval} = 1$	$M_{eval} = 3$	$M_{eval} = 5$
3DIEBench	None	3	80.91	81.61	86.05	87.36
3DIEBench	Rotation	1	84.88	84.08	85.34	85.31
3DIEBench	Rotation	3	82.49	81.72	86.14	87.41
3DIEBench	Rotation + Color	4	74.88	71.14	75.97	79.31
CIFAR100	None	2	53.00	51.60	57.05	58.37
CIFAR100	Crop + Jitter + Blur	1	56.23	54.24	52.90	52.92
CIFAR100	Crop + Jitter + Blur	2	52.07	53.07	59.34	60.35
CIFAR100	Crop + Jitter + Blur	3	46.31	49.48	57.60	58.33
CIFAR100	Crop	2	52.62	52.06	58.07	59.32
CIFAR100	Color Jitter	3	54.92	50.21	57.20	58.62
CIFAR100	Blur	3	51.41	48.69	55.54	56.72
Tiny ImageNet	None	2	32.84	30.48	35.03	35.97
Tiny ImageNet	Crop + Jitter + Blur	1	33.03	32.34	36.14	37.07
Tiny ImageNet	Crop + Jitter + Blur	2	27.20	30.57	34.99	35.56
Tiny ImageNet	Crop + Jitter + Blur	3	24.74	28.84	33.78	34.68
Tiny ImageNet	Crop	2	31.13	30.89	35.07	35.69
Tiny ImageNet	Color Jitter	3	31.85	29.05	34.27	35.21
Tiny ImageNet	Blur	3	27.20	28.83	34.82	35.79
STL-10	None	4	61.38	62.21	69.06	71.12
STL-10	Position	4	81.20	71.45	81.53	83.67
STL-10	Position (no saliency)	4	79.29	63.14	76.93	80.09
STL-10	Position (no IoR)	4	72.49	68.95	76.84	78.21

B.5. Visualization of UMAP projections for models without action conditioning

In Figure 13 we provide the UMAP projections for seq-JEPA representations trained on 3DIEBench but without action conditioning. Figure 14 shows UMAP projections for seq-JEPA representations trained on STL-10 via predictive learning across saccades without action conditioning. In these visualizations, the color gradients that implied high equivariance in UMAPs of action-conditioned models are either absent or less pronounced.

B.6. Transfer learning results on ImageNet-1k

In this section, we consider transfer learning on ImageNet-1k using our frozen model trained on STL-10 via predictive learning across saccades. We follow the same evaluation protocol as the in-distribution setting and train a linear probe on

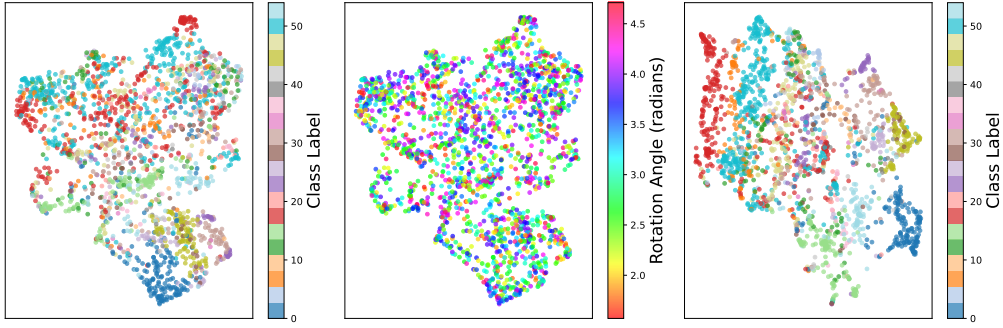


Figure 13: Visualization of 2-D UMAP projections of seq-JEPA’s encoder and aggregate representations. The model is trained on 3DIEBench without any action conditioning with $M_{tr} = 3$ and $M_{val} = 5$. Encoder representations for each view observation, color-coded by class category (**left**) and rotation angle (**middle**). The aggregate token representation for $M_{val} = 5$ observations during inference, color-coded by class category (**right**).

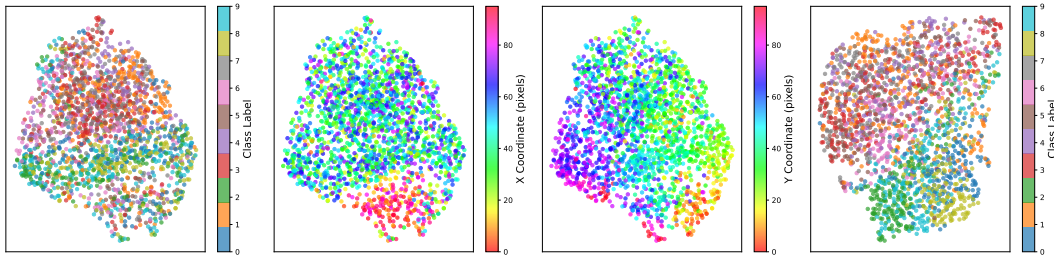


Figure 14: Visualization of 2-D UMAP projections of seq-JEPA’s encoder and aggregate representations. The model is trained on STL-10 via predictive learning across saccades with no action conditioning and with $M_{tr, val} = 4$. Encoder representations for each view observation, color-coded by class category (**left**) and X and Y pixel coordinates (**middle** panels). The aggregate token representation for $M_{val} = 4$ observation patches during inference, color-coded by class category (**right**).

ImageNet-1k training set and evaluate it on the validation set using the aggregate representation for different inference sequence lengths. We use DeepGaze-IIIE to extract saliency maps of ImageNet-1k, resize them to 224×224 , and use them to extract the foveated patches. Figure 15 shows the top-1 accuracy on ImageNet-1k for two different patch sizes (32 and 84). These results hint at the possibility of scaling seq-JEPA to larger data regimes by striking a trade-off between the patch size and sequence length. For example, using full-resolution 224×224 images, a forward pass through a ResNet-18 encoder takes approximately 1.83×10^9 flops, while a forward pass of seq-JEPA with the default transformer encoder, $M_{val} = 4$ and 84×84 patches takes 1.25×10^9 flops. Using the CIFAR variant of ResNet-18 with 32×32 patches and $M_{val} = 8$ requires 2.35×10^9 flops.

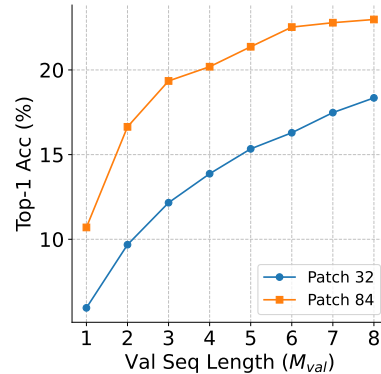


Figure 15: Linear probe transfer learning accuracy on ImageNet-1k for two different patch sizes; the model is trained on STL-10 via predictive learning across saccades.